Shelf Wave Scattering due to a Longshore Jump in Topography

JOHN F. MIDDLETON* AND DANIEL G. WRIGHT

Physical and Chemical Sciences, Department of Fisheries and Oceans, Bedford Institute of Oceanography, Dartmouth, Nova Scotia, Canada

(Manuscript received 25 March 1987, in final form 9 August 1987)

ABSTRACT

The scattering of barotropic shelf waves by an abrupt jump in longshore topography is examined for unbounded and bounded exponential shelves by matching modal representations for longshore transport and sea level. Estimates of the ratio of transmitted to incident energy flux, F_T/F_I, are obtained for a bounded shelf (i.e., with coastal and offshore walls) using an asymptotically exact first-order differential equation for streamfunction that is derived from the matching conditions at low frequencies. The equation is shown to represent the production of relative vorticity, manifest as backscattering waves, due to vortex stretching induced by flow over the jump. At low frequencies, low mode waves exhibit a strong tendency to propagate along f/h contours even as the jump is crossed and scattered energy is found to reside mainly in the gravest reflected and transmitted modes. Results agree with corresponding low frequency solutions derived using a direct mode-matching procedure. At higher frequencies the solutions determined using the mode matching procedure fail to conserve energy: possible explanations are discussed. For unbounded shelves a simple analytical expression for the ratio of transmitted to incident energy flux, F_T/F_I, is derived and used to show that (i) transmission decreases with increasing jump size, (ii) a topographic jump acts to pass (retard) incident modes which have cross-shelf scales that are larger (smaller) than that of the topography, (iii) F_T/F_I is a maximum and essentially constant at frequencies much less than that of the zero in incident wave group speed, σ_I, and (iv) that F_T/F_I monotonically decreases to zero as frequency approaches σ_I. These results also summarize the qualitative nature of the approximate solutions for a bounded shelf determined using the mode matching technique. The analysis suggests that results may be applicable to scattering by smooth jumps provided the longshore topographic scale is less than half the shelf width.

1. Introduction

The scattering of continental shelf waves by longshore variations in bottom topography has been the subject of several theoretical investigations over the past decade. Allen (1976), for example, showed that under the long-wave approximation shelf waves can be scattered into other forward propagating modes by small longshore variations in bottom topography. Where the long-wave approximation is not made, energy may be scattered into both forward and backward propagating modes and preferentially into the highest of modes if the topographic variation is manifest as a small isolated bump (Chao et al., 1979). The scattering of wave energy by an ensemble of small bumps was later considered by Brink (1980) and shown to result in a damping of the coherent wave field that may be comparable with that due to turbulent bottom friction.

The scattering by large longshore topographic variations was addressed with the long-wave approximation relaxed in the numerical study by Wang (1980). In particular, Wang found that little scattering results from the convergence/divergence of depth contours provided that the longshore topographic scale is of the order of the shelf width or greater. Such a result was also demonstrated by Hsueh (1980) and Davis (1983) for shelves where longshore variations in both depth and width occur in a self similar manner. More recently, however, Webster (1987) has shown that considerable wave scattering may occur if the longshore topographic scale is less than half the shelf width.

In this paper we shall consider the scattering by a large, abrupt change in depth, on a shelf that is otherwise uniform in the longshore direction and increases exponentially in the offshore direction (see Fig. 1). Such topography, while idealized, is perhaps exemplified by the Labrador Shelf where severe glaciation has resulted in a sequence of banks and saddles for which the depth may vary from 200 to 400 m in 90 km or about half the shelf width. In addition, the idealized topography will permit the streamfunction to be simply determined as a sum of wave modes on each side of the topographic jump, and matched assuming continuity of sea level and longshore transport. The mode matching techniques used are similar to those employed by Wilkin

* Present affiliation: School of Mathematics, University of New South Wales, P.O. Box 1, Kensington, N.S.W., Australia, 2033.

Corresponding author address: Dr. Daniel G. Wright, Dept. of Fisheries and Oceans, Bedford Institute of Oceanography, P.O. Box 1006, Dartmouth, Nova Scotia, Canada B2Y 4A2.

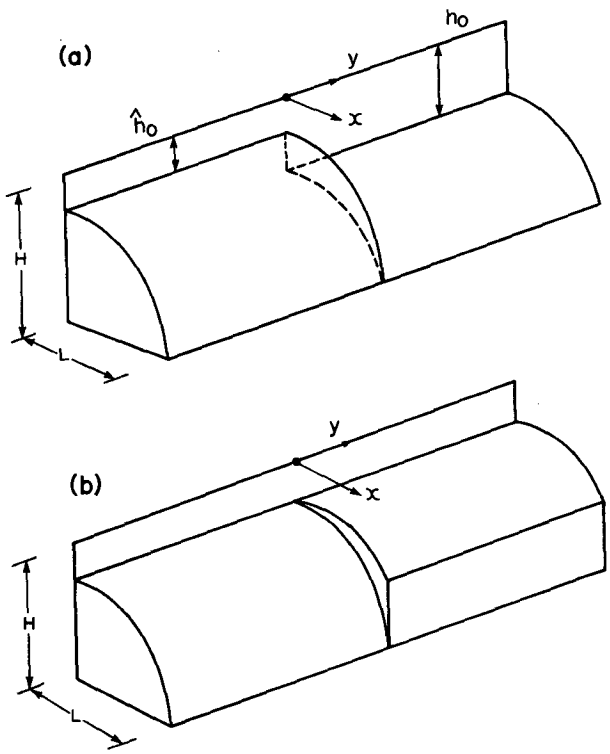

FIG. 1. Exponential shelf bathymetries for (a) a nearshore abrupt topographic jump and (b) a jump that is most abrupt at the offshore boundary. In the consideration of bounded shelf solutions, a wall which is not indicated is included at $x = L$.

and Chapman (1987) who examined the shelf wave scattering due to an abrupt increase in shelf width.

In section 2, wave mode solutions are obtained for exponential shelves that are either bounded by coastal and offshore walls or unbounded in both onshore and offshore directions. In section 3 the scattering by an abrupt topographic jump is examined for shelves which are bounded in cross-shore extent. At low frequencies, an asymptotically exact differential equation in streamfunction at the jump is derived and results for scattered wave amplitude and net transmitted energy flux are obtained for the case of an abrupt jump in shelf *depth*. These results are validated in section 4 where estimates of transmitted flux are obtained for frequencies up to that of the zero in group speed of the incident wave. The utility of the asymptotically exact differential equation is demonstrated again in section 5, where near exact, analytical results are obtained for the low frequency scattering due to an abrupt jump in shelf *width*. In section 6, the modal solutions appropriate to an unbounded shelf, in both on and offshore directions, are used to examine the scattering by both an abrupt and smooth topographic jump. The analytical results obtained provide further insight into scattering on the more realistic bounded shelf topographies as well as indicating the applicability of abrupt topographic results to situations where longshore depth variations occur over a finite distance.

In the following analysis we neglect the effect of stratification which, if sufficiently strong, may act to prevent all backscattering of energy through the effective elimination of the short wave modes, (see Huthnance, 1978; Chapman, 1983). The important restrictions which this places on the applicability of the results to stratified shelf regions will be discussed in section 7. However, an understanding of shelf wave scattering in a barotropic fluid would seem essential and, as will be seen, the results below provide a near analytical description of low frequency scattering by abrupt topography.

2. Modal solutions and fluxes

We consider barotopic wave propagation along a shelf where depth increases exponentially from the coast, located at $x = 0$,

$$h = \begin{cases} h_0 \exp(2bx) & y > 0 \\ \hat{h}_0 \exp(2\hat{b}x) & y < 0 \end{cases} \tag{2.1}$$

and where h_0, $\hat{h}_0$ and b, $\hat{b}$ may differ so that the longshore topographic variation is manifest as a jump at $y = 0$, (see Fig. 1). The depth parameters h_0, b, etc. will be specified below.

We define u and v to be cross and longshelf velocities so that with a rigid lid a transport streamfunction satisfying, $\Psi_x = hv$ and $\Psi_y = -hu$ may be introduced. The vorticity equation on either side of the jump may then be written as

$$[(\Psi_x/h)_x + h^{-1}\Psi_{yy}]_t - f\Psi_y(1/h)_x = 0 \tag{2.2}$$

where f, the Coriolis frequency, is assumed constant. The modal solutions to (2.2) are assumed to be of the separable, wavelike form

$$\Psi = \phi(x) \exp[i(ky - \omega t)], \tag{2.3}$$

where ω and k denote frequency and longshore wavenumber, and with (2.2) result in the differential equation for the cross-shelf amplitude:

$$(h^{-1}\phi_x)_x - (k^2 + 2bkf/\omega)h^{-1}\phi = 0 \tag{2.4}$$

where b should, of course, be replaced by $\hat{b}$ for $y < 0$.

a. *Modal solutions*

To solve (2.4), boundary conditions on Ψ and hence ϕ must be specified at both $x = 0$ and $x = L$. Here results will be presented using two distinct sets of boundary conditions, the first of which is obtained by imposing a wall at both the coast and offshore boundary at which the offshore transport, $hu = -\Psi_y$, must then vanish. The assumed solution (2.3) then implies that

$$\phi = 0 \quad \text{at} \quad x = 0, L \tag{2.5}$$

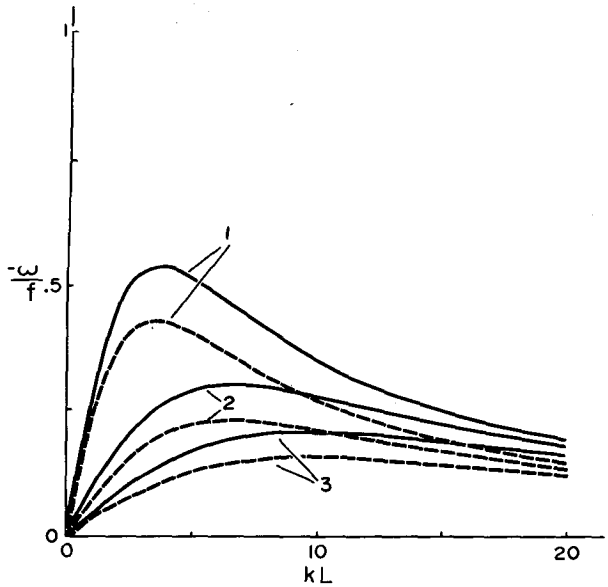

FIG. 2. Dispersion curves obtained from (2.8) assuming a wall at the shelf break and the slope parameters $b = 2L^{-1}$ (solid) and $b = 1.5L^{-1}$, (dashed). The first three modal curves are numbered and the cross-shelf wavenumber m is a multiple of π.

and with (2.4), leads to an infinite number of modal solutions of the form

$$\phi = h^{1/2} \sin mx \tag{2.6}$$

where an arbitrary constant, with dimension $L^2H/$(time), has been suppressed,

$$m = j\pi L^{-1}, \quad j = 1, 2, 3, \cdots \tag{2.7}$$

$$k^2 + 2bkf/\omega + m^2 + b^2 = 0. \tag{2.8}$$

The dispersion relation (2.8) implies that there exists, for each mode (or value of j), two wavenumbers given by

$$k^{\mp} = -\omega^{-1}fb[1 \mp (1 - \omega^2\sigma^{-2})^{1/2}] \tag{2.9}$$

where

$$\sigma = -f(1 + m^2/b^2)^{-1/2} \tag{2.10}$$

denotes the frequency of zero group speed, where $\partial\omega/\partial k = 0$ and $k^- = k^+$. (We shall adopt the convention that the wavenumbers, $k^{\mp}$, are positive so that, by (2.9) ω is negative for $f > 0$). For $|\omega| < |\sigma|$, the wavenumbers $k^{\mp}$ are real and distinct, (see Fig. 2) and correspond to long (−) and short (+) propagating waves. For $|\omega| > |\sigma|$ the wavenumbers $k^{\mp}$ become complex so that modes are evanescent and either grow or decay in the longshore direction.

The assumption of an offshore wall, leading to (2.7), is unrealistic although the dispersion curves and wave characteristics so obtained are similar to those found when a finite, depth H, ocean is imposed beyond $x = L$ (Wilkin and Chapman, 1987). Indeed, for the finite depth ocean case, the modal solutions on the shelf are again given by (2.6) while beyond $x = L$, $\phi = H^{1/2} \sin(mL) \exp[-k(x - L)]$, (see Buchwald and Adams, 1968). However, solutions for wave scattering by a topographic jump may *not* be obtained by matching series solutions consisting solely of such modes since for $x \geqslant L$, the gravest exponential mode, with smallest k, will dominate all others present. Presumably, the complete solution will involve additional modes, which are not of the separable form considered.

In the subsequent analysis we shall exploit the low frequency properties of the modal solutions (2.6) and wavenumbers m and k from (2.7) and (2.8). We note here that the cross-shelf momentum balance, $u_t - fv = -g\eta_x$, or $\eta_x = (gh)^{-1}[k\omega\Psi + f\Psi_x]$, will become independent of ω if the low frequency limit condition

$$\omega^2/\sigma^2 \ll 1 \tag{2.11}$$

is satisfied. The long waves become geostrophically balanced since from (2.9) $|\omega k\bar{V}| \ll fb$ so that, $\eta_x \approx (gh)^{-1}f\Psi_x$. The short wave momentum balance, while not geostrophic, is also independent of ω since $\omega k^+ \approx -2bf$ so that $\eta_x \approx (gh)^{-1}[f\Psi_x - 2bf\Psi]$. These asymptotic forms will be exploited in section 3 where scattered wave solutions are obtained at low frequencies by matching modal representations for longshore transport and sea level gradient, η_x.

The second set of boundary conditions considered corresponds to a disturbance on an exponential shelf that extends to infinity in both on and offshore directions. No coastal or shelf break conditions are assumed so that m is no longer discrete or dependent on ω. Solutions to the vorticity equation (2.2) may be written as

$$\Psi = h^{1/2}(x) \int_{-\infty}^{\infty} Q(m, k) \exp[i(mx + ky - \omega t)]dm \tag{2.12}$$

provided k is related to m by the dispersion relation (2.8). The utility of these somewhat unrealistic conditions and topography will become apparent in section 6 where (2.12) will permit a simple analytical exploration of shelf wave scattering by both an abrupt and a smooth topographic jump.

b. *Energy fluxes*

Of particular interest here will be the time-averaged net longshore energy flux defined by

$$F = \tfrac{1}{4}\rho g \int_R h(v^*\eta + v\eta^*)dx \tag{2.13}$$

where the asterisk denotes a complex conjugate and R the cross-shelf section of interest. Where the shelf is bounded at $x = L$ by a wall, a net flux over $[0, L]$ due to each propagating mode may be determined from (2.13) and written as

$$F = \frac{1}{2}\rho B(\omega k + fb) \tag{2.14}$$

where

$$B = \int_0^L h^{-1}\phi^2 dx. \tag{2.15}$$

The net flux due to each evanescent mode may be shown to vanish using the orthogonality properties of (2.4). In addition, at sufficiently low frequencies, where the condition (2.11) applies, the flux due to the long (−) and short (+) waves become equal and opposite and may be approximated by

$$F_{\mp} = \mp\frac{1}{2}\rho bfB \tag{2.16}$$

since, again, $\omega k^+ \approx -2bf$ and $|\omega k^-| \ll bf$.

Finally, the net flux corresponding to the unbounded shelf solution (2.12) may also be determined from (2.13) and written as

$$F = -\rho\pi \int_{-\infty}^{\infty} [\omega k + bf]QQ^* dm \tag{2.17}$$

where $k = k(m)$ is real and given by (2.9). If k is complex, corresponding to evanescent waves, the bracketed term in (2.17) should be replaced by $\frac{1}{2}[\omega(k + k^*) + 2bf]$ which from (2.9) is zero so that again only propagating modes may contribute to the net flux.

3. Low frequency solutions for a jump in depth

For the case where the shelf is bounded at $x = L$ by a wall, asymptotically exact solutions may be obtained at low frequencies by matching both sea level and longshore transport. The solutions for Ψ on either side of the jump will consist of an infinite sum of the discrete modal solutions, (2.6) and the condition for continuity of Ψ at $y = 0$ may be written as

$$\phi_I + \sum_{j=1}^{\infty} a_j\phi_j - \sum_{j=1}^{\infty} \hat{a}_j\hat{\phi}_j = 0 \tag{3.1}$$

where ϕ_I, ϕ_j and $\hat{\phi}_j$ denote incident, reflected and transmitted waves respectively and a_j, $\hat{a}_j$ are undetermined coefficients.

Sea level may be matched to within a time dependent constant (say $Ce^{-i\omega t}$) by matching η_x. The constant C represents the difference in the amplitudes of Kelvin waves which may exist on either side of the jump but which are of little interest here, as their associated velocities and energy fluxes are zero under the rigid-lid approximation. The condition for matching η_x may also be written as a sum of modal contributions

$$\eta_{Ix} + \sum_{j=1}^{\infty} a_j\eta_{jx} - \sum_{j=1}^{\infty} \hat{a}_j\hat{\eta}_{jx} = 0 \tag{3.2}$$

where

$$\eta_{jx} = (gh)^{-1}[k_j^+\omega\phi_j + f\phi_{jx}] \tag{3.3}$$

and so on.

Now at the low frequencies of interest here, we shall assume that the dominant reflected and transmitted modes in (3.1) and (3.2) are propagating rather than evanescent, since an increasingly large number of the former are available to match both sea level and transport as ω/f vanishes. The reflected propagating waves become extremely short at low frequencies, and if $\omega^2/\sigma^2(m)$ is small for each mode of significant amplitude, then as shown in section 2, $\omega k_j^+ \approx -2bf$ and $\eta_{jx} \approx (gh)^{-1}f[\phi_{jx} - 2b\phi_j]$. The incident and transmitted waves, on the other hand, become very long and geostrophically balanced so that $\eta_{Ix} \approx (gh)^{-1}f\phi_{Ix}$, and so on. The condition (3.2) may now be rewritten as

$$h^{-1}\{\phi_{Ix} + \sum_{j=1}^{\infty} a_j(\phi_{jx} - 2b\phi_j)\} = \hat{h}^{-1}\sum_{j=1}^{\infty}\hat{a}_j\hat{\phi}_{jx} \tag{3.4}$$

and with (3.1) is independent of frequency as $\phi_I(x)$, $\phi_j(x)$ etc. depend only on cross shelf wavenumbers which are simply multiples of π for a bounded shelf. Further, upon rearrangement, (3.1) and (3.4) yield the first-order differential equation in *total* streamfunction, ϕ, at $y = 0$

$$(1/h - 1/\hat{h})\phi_x = 2b(\phi - \phi_I)/h \tag{3.5}$$

which may be simply solved once h, $\hat{h}$, b and ϕ_I are specified!

To interpret this remarkable result, we note that the linearized vorticity balance

$$\underbrace{[(\Psi_x/h)_x + (\Psi_y/h)_y]_t}_{\text{(a)}} = f\underbrace{[\Psi_y(1/h)_x - \Psi_x(1/h)_y]}_{\text{(b)}}$$

will be dominated by the terms (a) and (b) in the vicinity of the jump since these involve the derivative, h_y, which is infinite at $y = 0$. Integration of these terms, from $y = -\epsilon$ to $+\epsilon$ results in

$$-f\Psi_x[1/h]_{-\epsilon}^{+\epsilon} = [\Psi_{yt}/h]_{-\epsilon}^{+\epsilon} \tag{3.5a}$$

where the left-hand side may be clearly identified with that in (3.5), and represents the net production of relative vorticity by flow across the jump. The right-hand side of (3.5a) represents the rate of change of relative vorticity, and will be dominated by the reflected wave modes since the incident and transmitted waves are very long at the low frequencies assumed: $\Psi_{yt} \sim \omega k^+\Psi \gg \omega k^-\Psi$. Further, for each reflected mode we have, $\omega k^+ \approx -2bf$, so that the right-hand side of (3.5a) may be written as $[\Psi_{yt}/h]_{-\epsilon}^{+\epsilon} \approx -2bf\Psi_R/h$ where Ψ_R denotes the total reflected wave streamfunction at $y = +\epsilon$ and is equal to $\phi - \phi_I$. The right-hand side of (3.5a), $-2bf(\phi - \phi_I)/h$, may now be identified with that in (3.5) which thus represents the rate of change of relative vorticity of the reflected waves, due to production by flow over the jump.

Solutions for ϕ obtained from the vorticity balance, (3.5), will also permit immediate determination of the net transmitted energy flux since from (2.14) and (2.15) we may write

$$F_T = -\frac{1}{2}\rho \hat{b} f \int_0^L \hat{h}^{-1}\phi^2 dx. \tag{3.6}$$

In addition, the first N coefficients a_j, $\hat{a}_j$, and hence total streamfunction, $\Psi(x, y, t)$ may be determined by solution of the system of equations that result from taking the inner product of (3.1) with $h^{-1}\phi_j$ and $\hat{h}^{-1}\hat{\phi}_j$. For example, where a wall is assumed at $x = L$, and all modes are orthogonal, the a_k, $\hat{a}_k$ are given by

$$\hat{a}_k = \left\{\int_0^L \hat{h}^{-1}\hat{\phi}_k^2 dx\right\}^{-1} \int_0^L \hat{h}^{-1}\phi\hat{\phi}_k dx \tag{3.7}$$

etc., and Ψ is reconstructed from

$$\Psi = \begin{cases} \phi_I \exp[i(k_I^- y - \omega t)] + \sum_{j=1}^{N} a_j\phi_j \\ \qquad \times \exp[i(k_j^+ y - \omega t)], \quad y \geq 0 \\ \sum_{j=1}^{N} \hat{a}_j\hat{\phi}_j \exp[i(\hat{k}_j^- y - \omega t)], \quad y \leq 0. \end{cases} \tag{3.8}$$

Inspection of (3.5) and (3.7) also shows that if ϕ_I is real, then so must be ϕ, a_j and $\hat{a}_j$ so that the incident, reflected and transmitted waves must be either in or out of phase with each other.

a. Results for a nearshore jump: Propagation from deep to shallow water

Here the backward ($y > 0$) and forward ($y < 0$) topographic parameters in (2.1) are chosen such that

$$h = H\exp[2b(x - L)], \quad \hat{h} = H\exp[2\hat{b}(x - L)], \tag{3.9}$$

so that the jump is most abrupt at the coast and vanishes at $x = L$, (see Figs. 1a or 3a, b).

The slope parameter $\hat{b}$ is assumed larger than b, so that the incident wave propagates from deep to shallow water. With (3.9), Eq. (3.5) may be integrated to yield

$$\phi(x) = \phi_I\hat{h}/h - hK^{-d}\int_0^x K^d(r)[\hat{h}(r)h^{-2}(r)\phi_I(r)]_r dr \tag{3.10}$$

where

$$K(x) = h\hat{h}^{-1} - 1$$

and $d = (1 - \hat{b}/b)^{-1}$ is negative. The function $K^{-d}(x)$ vanishes at $x = L$ and will dominate the integral involving $K^d(r)$ as x approaches L so $\phi \neq 0$ at $x = 0$ and L as required. [Note that $K^d(r) \sim [2(b - \hat{b})]^d(r - L)^d$ near $r = L$ while the remainder of the integrand in (3.10) is a bounded function of r. The second term in (3.10) is thus $O(x - L)$ near $x = L$.] For a vanishingly small topographic jump, where $h \approx \hat{h}$, nearly perfect transmission results and $\phi(x) \approx \phi_I(x)$. On the other hand, where $\hat{b} \gg b$, the integration in (3.10) may be immediately performed to show that $\phi(x) \approx 0$ corresponding to perfect reflection by a wall (see Fig. 3a).

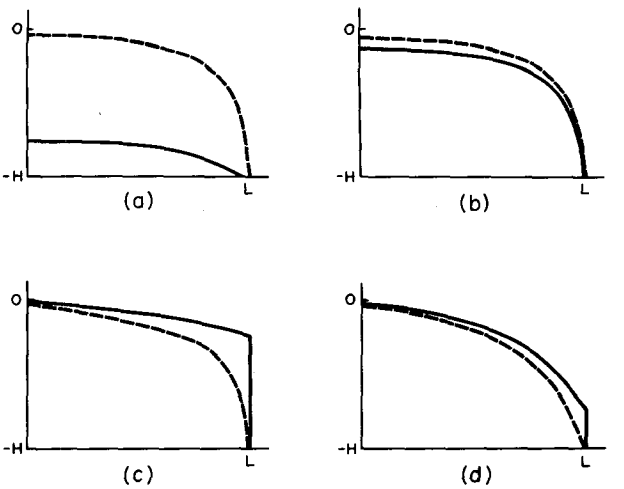

FIG. 3. Profiles of the bathymetry shown in Fig. 1 where for (a) and (c) the jump size from backward (solid) to forward (dashed) topography is large and $\hat{b} \gg b \sim O(1)$. In (b) and (d) both slope parameters are large of similar order and the topographic jump effectively small.

For illustrative purposes, we have determined the total streamfunction $\Psi(x, y, t)$ from (3.7)–(3.10) for the case of a wall at $x = L$ and an incident first mode wave. All integrations were accomplished using the rectangle rule and 1000 subdivisions of the interval, $[0, L]$. The slope parameter values $\hat{b} = 2b = 2L^{-1}$ were assumed and at the frequency $-0.1f$ chosen, there exist six transmitted and three reflected propagating waves. The number of propagating waves here is certainly not large, and with the amplitudes a_j, $\hat{a}_j$ determined from (3.7), may be insufficient to fully represent the solution for ϕ that is only asymptotically valid as ω/f vanishes, and formally given by an infinite sum of modes. A measure of this truncation error is given by

$$\left\{\int_0^L 4\phi^2 dx\right\}^{-1/2}\left\{\int_0^L (2\phi - \phi_I - \sum a_j\phi_j - \sum \hat{a}_j\hat{\phi}_j)^2 dx\right\}^{1/2} \tag{3.11}$$

where the sums are only over the wave modes which exist at the chosen frequency. For $\omega = -0.1f$, an error of less than 2% was indicated by (3.11) so that the solutions presented are apparently valid. In addition, most scattered energy was found to reside in the two gravest reflected and transmitted modes, suggesting that the (neglected) contribution to Ψ made by the evanescent modes may be ignored. Indeed this will be shown in section 4 (see also Wilkin and Chapman, 1987) where both propagating and evanescent modes are included in the representation for $\Psi(x, y, t)$.

The amplitude of the streamfunction obtained by

the method outlined above is plotted in Fig. 4. We note the apparent tendency for waves to propagate along f/h contours even as the jump is crossed. All f/h contours in the region $y \geq 0$ are continued across the jump, and as shown a region of quiescence exists on the forward ($y < 0$) side where incident wave energy is unable to propagate. The reflection due to the jump is marked, and the $0.6L$ wavelength pattern shown is primarily due to interference between the incident and two gravest reflected modes which have wavelengths of around $1.1L$ and $0.3L$ respectively. The two gravest reflected waves (and second mode transmitted wave) were also found to be out of phase with the incident and gravest transmitted waves. The ratio of total transmitted to incident energy flux was estimated at 0.38. Fluxes were estimated individually for the first three reflected waves, $(0.565, 0.037, 0.009)F_I$ and transmitted waves, $(0.259, 0.099, 0.014)F_I$ and show that most energy is scattered into the gravest modes. Indeed, the first two gravest transmitted and reflected waves account for more than 93% of the total transmitted and reflected fluxes, respectively.

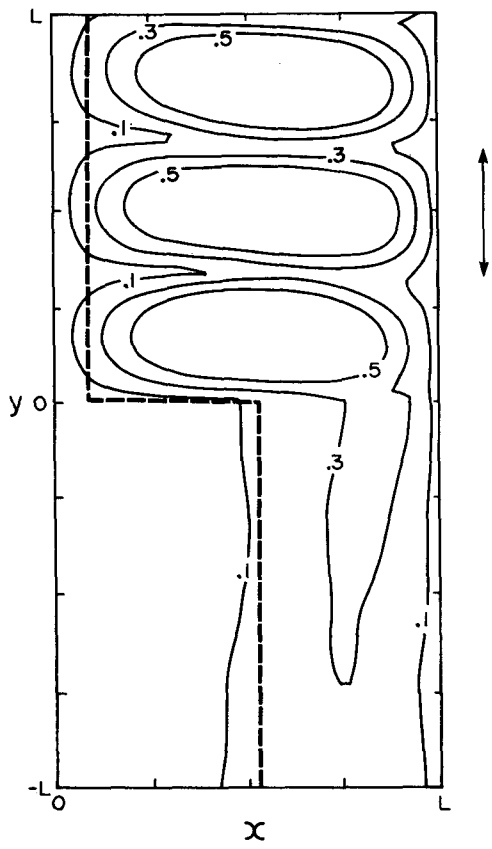

FIG. 4. Streamfunction amplitude for the scattering of a first-mode incident wave by a nearshore jump (Fig. 1a) with a wall at $x = L$. Contour values have been normalized by the incident wave amplitude and the results were obtained from (3.7)–(3.10) for a frequency of $\omega = -0.1f$ and the slope parameters $\hat{b} = 2b = 2L^{-1}$. The tendency for waves to propagate along the dashed f/h contour is apparent as is the strong reflection by the jump. The vertical arrow indicates the first reflected mode wavelength.

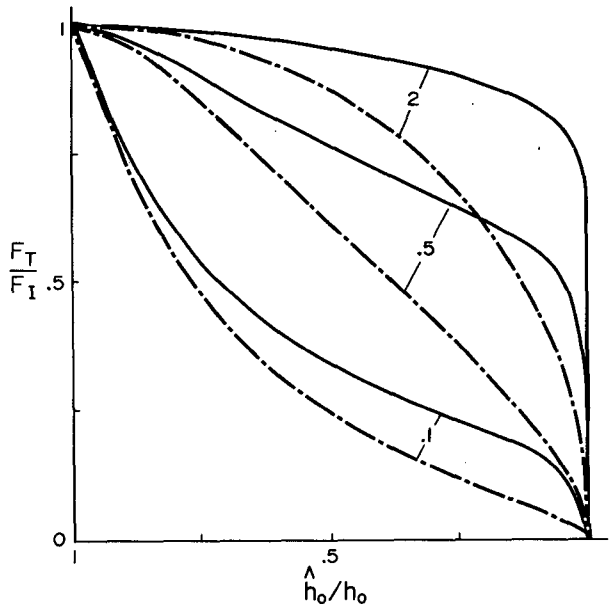

FIG. 5. The flux ratio F_T/F_I *vs* the nearshore jump size $\hat{h}_0/h_0$ for the scattering of a low frequency, first mode wave with a wall at $x = L$. These results (dot-dashed) were obtained from (3.10) for the backward slope parameters, bL, indicated and may be compared with those, (solid), for the scattering by an offshore jump: in the latter case the horizontal axis should be relabeled as $\hat{h}(L)/h(L)$.

As an initial examination of the sensitivity of transmitted flux to the details of the topography, solutions for ϕ were also obtained for the slope parameters $bL = 0.1$, 0.5 and 2 using first mode incident waves, and results for the ratio of transmitted to incident flux, F_T/F_I, are presented in Fig. 5. Apparent from the figure is a general decrease in transmission as jump size increases and, where $\hat{h}_0/h_0$ is near zero, the forward side topography becomes wall-like (Fig. 3a), and total reflection obtains. The results also show an increase in F_T/F_I with the slope parameter b, as the effective jump size becomes smaller and the shelf depth at the coast $h_0 = He^{-2bL}$ vanishes (see Fig. 3b).

Results for the scattering of second and third mode incident waves have also been determined for the slope parameter $bL = 0.5$. The estimates of F_T/F_I obtained are presented in Fig. 6 and show a decrease in transmission as mode number is increased so that a topographic jump acts to low pass the gravest mode waves, where m is smallest.

b. Results for an offshore jump: Propagation from shallow to deep water

The preceding solutions were obtained for a topography, (3.9), for which all f/h contours in the backward region are continued across the jump. However, if $\hat{h}_0/h_0$ is chosen to be greater than one, so that waves

now propagate from shallow to deep, all f/h contours are not continued across the jump and the solution (3.5) becomes unbounded at $x = L$. (The function $K(x)$ again vanishes at $x = L$, but since $d = (1 - \hat{b}/b)^{-1}$ is now positive, the term $K^{-d}(x)$ in (3.10) becomes infinite while the integral remains finite.) Possibly the solution fails because some f/h contours now disappear into the coast so that some fluid columns are left without a rest position after crossing the jump. In addition, no gravity waves exist to permit geostrophic adjustment of the new "unbalanced" state, and no wavelike solution of the form assumed here seems possible.

Solutions for wave propagation from shallow to deep water may still be found, but with a topography now given by

$$h = H \exp[2b(x - L)], \quad \hat{h} = H \exp[2\hat{b}x - 2bL] \tag{3.12}$$

where $\hat{b} > b$. The maximum jump occurs offshore, (Figs. 1b and 3c, d), and all f/h contours in the region $y > 0$ are continued across $y = 0$. Solutions to (3.5) may be obtained and written as

$$\phi(x) = \hat{h}\phi_I/h - hK^{-d} \int_L^x K^d(r)[\hat{h}(r)h^{-2}(r)\phi_I(r)]_r dr \tag{3.13}$$

where

$$K(x) = 1 - h\hat{h}^{-1}$$

and d is again given by $(1 - \hat{b}/b)^{-1}$ and is negative. In obtaining (3.13) we have integrated from $x = L$ so as to avoid the singularity in $K^d(x)$ at $x = 0$ and used the fact that $\phi(L) = \phi_I(L) = 0$ for a wall at $x = L$. (We also note that the solution (3.13) is unbounded for $\hat{b} < b$ where all f/h contours are not continued across the jump.) The solution (3.13) satisfies the coastal boundary condition, $\phi(0) = \phi_I(0) = 0$, since the second term in (3.13) is $O(x)$ near $x = 0$.

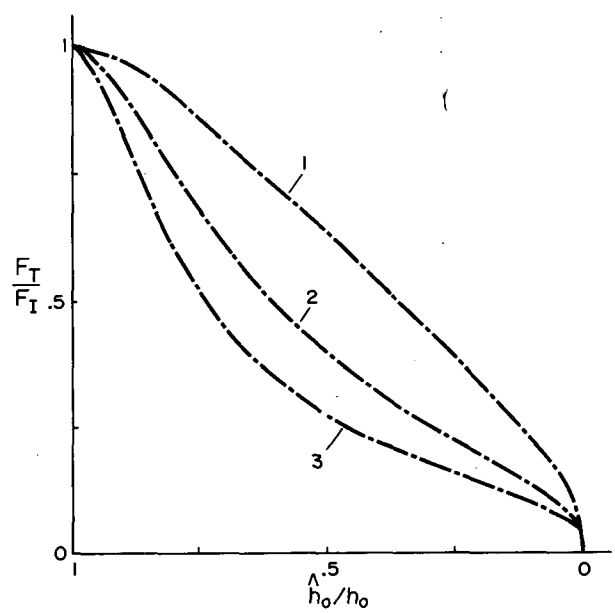

FIG. 6. As in Fig. 5 but for second and third mode incident waves on a bounded shelf. The backward slope parameter is fixed at $b = (2L)^{-1}$.

Results for the ratio F_T/F_I were obtained from (3.13), (Fig. 5), and again show a decrease in transmission as jump size increases and $h(L)/\hat{h}(L)$ becomes small (see Fig. 3c). The ratio F_T/F_I also increases with b since wave propagation is eased over a smaller jump (Fig. 3d). Results for propagation from deep to shallow or shallow to deep water are qualitatively consistent but it is apparent from Fig. 5 that transmission for a given jump size, $\hat{h}_0/h_0 = h(L)/\hat{h}(L)$, is generally greater for the case of an offshore jump than for a jump at the coast. This is consistent with the results of Chao et al. (1979) who showed that small topographic features near the coast scattered wave energy more effectively than a similar feature offshore.

4. A direct mode matching approach for arbitrary frequencies

Here we shall examine the scattering of a first mode incident wave by a topographic jump which is most abrupt at the coast (Fig. 1a), with a wall at the shelf break. As we shall no longer demand that ω/f be small, the matching conditions (3.1) and (3.2) may not be rearranged to yield a differential equation in total streamfunction, ϕ, at $y = 0$. Further, few propagating waves may exist so that those which are evanescent, and decay away from the jump, will be important in the modal representation, (3.8), for $\Psi(x, y, t)$. We shall assume here that Ψ on either side of the jump may be adequately represented by the 20 gravest propagating and evanescent modes and seek to determine the coefficients a_j, $\hat{a}_j$ by minimizing the sum of squares of matching conditions

$$R^2 = \int_0^L \{|3.1|^2 + w|3.2|^2\}dx \tag{4.1}$$

with respect to each a_j and $\hat{a}_j$. The parameter w was chosen as

$$w = \left\{\int_0^L \eta_{Ix}{}^2 dx\right\}^{-1} \int_0^L \phi_I{}^2 dx \tag{4.2}$$

so that similar weight is given to both matching conditions; the following results were found to be insensitive to arbitrary order of magnitude variations in w.

The least-squares procedure above differs somewhat from other mode fitting techniques (Yeh, 1975; Wilkin and Chapman, 1987) where a unique set of equations for a_j, $\hat{a}_j$ may be obtained by taking the inner product of the matching conditions with the modes, $h^{-1}\phi_j$ and $\hat{h}^{-1}\hat{\phi}_j$. The choice of inner product in these analyses is unambiguously dictated by a change in domain size. Here, however, both matching conditions and modes pertain over the same domain, $[0, L]$, and no unique choice of inner product is evident. Indeed, solutions

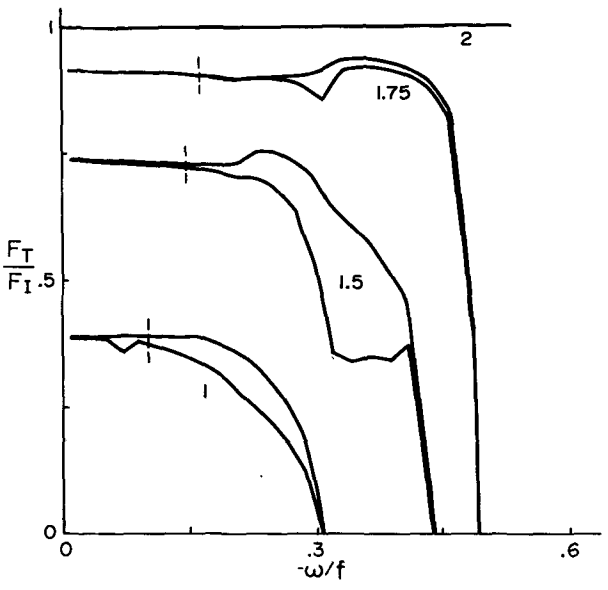

FIG. 7. The ratio F_T/F_I for the scattering of a first mode wave by a nearshore jump with a wall at $x = L$. Results for both F_T/F_I (lower curve) and $(F_R + F_I)/F_I$ (upper curve) were determined by minimizing (4.1) and the difference indicates the net error in the estimated fluxes for each of the indicated slope parameters, bL. At frequencies below $\sigma_I/3$ (the vertical dash), the errors are small and results for F_T/F_I near constant and equal to those that may be obtained from (3.10). In all cases, $\hat{b}L = 2$, and perfect transmission results when $b = \hat{b}$ and no jump exists.

for first-mode scattering by the topographic jump shown in Fig. 1a, were obtained using several combinations of inner product, but all found to be grossly in error in either one or both matching conditions.

Solutions were obtained, however, by minimizing (4.1) for the case of an incident first-mode wave propagating from deep to shallow water (Fig. 1a) for which all f/h contours in the region $y \geq 0$ are continued across the jump: the obtained matches for Ψ and η_x were found to be accurate to within 2%. Continuity of f/h contours again seems necessary since solutions obtained with the nearshore jump topography were found to be grossly in error for the converse case of wave propagation into deepening water. Thus, results are only presented for the former case. Estimates of the 40 coefficients a_j, $\hat{a}_j$ were determined for the three sets of slope parameters $L(b, \hat{b}) = (1, 2)$, $(1.5, 2)$ and $(1.75, 2)$ and at 20 frequencies between $-0.01f$ and $\sigma_I \equiv \sigma(m_I)$, the frequency of zero group speed of the incident wave. The total reflected and transmitted energy fluxes were then obtained from (2.14) and results for F_T/F_I, and $(F_I + F_R)/F_I$ are presented in Fig. 7 where the difference in the pairs of curves corresponds to the normalized error, $(F_I + F_R - F_T)/F_I$.

As shown, the errors while small at low frequencies, are somewhat larger at frequencies above $\sigma_I/3$. Small errors are not manifest in the 2% accurate matches obtained for Ψ and η_x in part because these quantities are determined from a large sum of coefficients, a_j, $\hat{a}_j$, while the fluxes are determined from only those which pertain to the (few) propagating waves. However, no reduction in flux error was found upon doubling the total number of modes present, suggesting that the solution for Ψ, at frequencies above $\sigma_I/3$ may not be exactly represented by a sum of the separable wave modes assumed here. Inclusion of the Kelvin wave mode, $\eta = Ce^{-i\omega t}$, through matching η rather than η_x in (4.1) was also found *not* to reduce the errors in the flux estimates. This result is puzzling, since Wilkin and Chapman (1987) have shown the Kelvin wave mode to be important in the conservation of energy for scattering by an abrupt jump in shelf width. Further, minimization of (4.1) subject to the constraint that the net energy flux be equal on either side of the jump produced unacceptable root-mean-square errors ($\sim$10%) in η_x and Ψ at the middle-range frequencies where Fig. 7 indicates problems. Clearly at higher frequencies there is some basic problem with either the assumed physics or the variety of mode matching solution techniques tried (see section 7 for further discussion). Although we cannot state conclusively what the source of the problem is, the fact that near exact solutions do not seem possible for such an apparently tractable problem, is in itself noteworthy.

With a caveat on the high frequency results, it is apparent from Fig. 7 that the transmitted energy decreases with increasing frequency and in agreement with the results of Wang (1980), at $\omega = -\sigma_I$ total reflection results since the first mode incident and reflected waves are then identical in both cross and long-shelf structure. In general F_T/F_I increases as the jump size is decreased, and where $b = \hat{b}$ perfect transmission must result, at all frequencies below σ_I.

While we have commented in detail upon the validity of the high frequency results, it should also be noted that the errors in total flux are, in general, small at frequencies below $\sigma_I/3$ and indeed vanish as ω approaches zero. In this parameter range, the estimates of F_T/F_I are nearly constant, independent of frequency and in fact equal to those that may be obtained from the differential equation (3.5). The results obtained here, for $\omega = -0.1f$ and $\hat{b}L = 2bL = 2$, may also be compared with the coefficients, a_j, $\hat{a}_j$ and streamfunction determined from the differential equation (3.5). Remarkably, the coefficients a_j, $\hat{a}_j$ of the propagating waves obtained from both (3.5) and (4.1) were found to be within 1% of each other and the streamfunction pattern in Fig. 4 indistinguishable from that based upon the 40 propagating and evanescent modes assumed here. Such agreement at low frequencies is a result of the dominance of Ψ by the gravest propagating modes. Indeed, the amplitudes of the evanescent modes were found here to be an order of magnitude less than those of the gravest propagating waves, suggesting that the latter are most readily excited by wave scattering. Similar results were also found by Wilkin and Chapman

(1987) for wave scattering by an abrupt increase in shelf width and are in contrast with scattering by small isolated bumps, where the highest propagating modes are excited, (Chao et al., 1979).

5. Low frequency solutions for a jump in shelf width

In a recent paper, Wilkin and Chapman (1987) examined the scattering due to an abrupt jump in shelf *width* using a mode matching technique essentially as outlined in section 4. Here we show that many of the low frequency results obtained by these authors may be obtained analytically from the differential equation (3.5).

Following Wilkin and Chapman (1987), the shelf depth is assumed continuous in the longshore direction and the coordinate system is reoriented so that the origin lies at the offshore boundary, with y directed "dowmstream" and x directed towards the coast. At $y = 0$, the shelf is assumed to widen abruptly from $x = L_1$ to $x = L_2$ and the depth is given by $h = h_0 \exp(-2bx)$ for all y.

Now since there can be no flow through the cross-shelf wall between $x = L_1$ and $x = L_2$, the total streamfunction must vanish there. In addition, since depth is continuous, $h \equiv \hat{h}$, equation (3.5) implies that $\phi = \phi_I$ between $x = 0$ and $x = L_1$ so that the total streamfunction of the transmitted waves is given by

$$\phi = \begin{cases} \phi_I, & 0 < x \leqslant L_1 \\ 0, & L_1 \leqslant x \leqslant L_2, \end{cases} \tag{5.1}$$

and no backscattered waves exist.

With a wall at $x = 0$ (the offshore boundary), the jth incident and transmitted modes are given by $h^{1/2} \times \sin(j\pi x/L_1)$ and $h^{1/2} \sin(j\pi x/L_2)$. The amplitudes $\hat{a}_j$ of each transmitted mode may be determined for an arbitrary incident wave field since

$$\phi = \sum \hat{a}_j \hat{\phi}_j$$

and (5.1) together imply that

$$\hat{a}_j = \left\{ \int_0^{L_2} \hat{h}^{-1} \hat{\phi}_j^2 dx \right\}^{-1} \int_0^{L_1} \hat{h}^{-1} \hat{\phi}_j \phi_I dx. \tag{5.2}$$

The preferential excitation of modes whose cross-shelf structure is similar to that of ϕ_I is immediately apparent. Further, it is obvious from (5.2) that $\hat{a}_j$ is independent of b so that the steepness of the topography enters only through the structure of the eigenfunctions.

For the example of a first mode incident wave, (5.2) reduces to

$$\hat{a}_j = \frac{\mu}{j\pi} \{\sin[\pi(\mu - 1)]/(\mu - 1) - \sin[\pi(\mu + 1)]/(\mu + 1)\}$$

where $\mu = jL_1/L_2$. With $L_2/L_1 = 2.25$, the amplitudes of the seven transmitted propagating waves are given by [0.347, 0.461, 0.315, 0.084, 0.046, 0.040, 0.011] which may be compared with the values [0.346, 0.461, 0.316, 0.085, 0.047, 0.043, 0.013] obtained by Wilkin and Chapman (1987), Table 1, who chose $\omega = -0.1f$, $bL_1 = 1.0$ and allowed for some 40 propagating and evanescent waves in their mode matching procedure. As shown in section 4, and by Wilkin and Chapman (1987), the evanescent wave amplitudes are relatively small at low frequencies and so contribute little to the total solution for $\Psi(x, y, t)$. For the example above, $\Psi(x, y, t)$ may be immediately reconstructed using (3.8) and the seven dominant modal amplitudes determined above.

Finally, we note that in the preceding case, all f/h contours in the backward region are continued across the jump in shelf width. Solutions may not, however, be obtained from (3.5) for the converse case of a narrowing shelf, $L_2 < L_1$, since evanescent waves would clearly be required to satisfy $\phi = 0$ along the wall at $y = 0$, $L_2 < x < L_1$. For this case we note that not all f/h contours in the backward region, are continued past the jump in width, since some will terminate at the cross-shelf wall. Remarkably, Wilkin and Chapman (1987) have obtained accurate low frequency solutions for such topography (their Fig. 3), although they dismiss them as unrealistic since short waves (which do not exist for typical stratification conditions on shelves) are required by the solution. Nevertheless, the existence of solutions in a case for which f/h contours in the backward shelf region are not continued across the jump is interesting.

6. Unbounded shelf solutions

a. Results for an abrupt topographic jump

Presented below are exact analytical solutions for the scattering of a spectrum of propagating, long waves incident on an abrupt jump in longshore topography. In particular, the topographic scales on either side of the jump, h_x/h and $\hat{h}_x/\hat{h}$, are assumed identical and equal to $2b$, so that from (2.1), the jump size is a constant fraction of depth and given by

$$s = \hat{h}_0/h_0. \tag{6.1}$$

We envisage some wave source at $y \gg 0$ so that both the incident and transmitted streamfunctions will be composed of long waves, for which k^- and m are related by the dispersion relation (2.9), $k^- = k^-(m)$. The reflected streamfunction will, on the other hand, be composed of short waves only for which $k^+ = k^+(m)$. The streamfunction solution for incident (I), reflected (R) and transmitted (T) waves can be written as

$$\Psi_I = h^{1/2}(x) \int_{-\infty}^{\infty} Q_I(m, k^-) \exp[i(mx + k^- y - \omega t)] dm$$

$$\Psi_R = h^{1/2}(x) \int_{-\infty}^{\infty} Q_R(m, k^+) \exp[i(mx + k^+ y - \omega t)] dm \tag{6.2}$$

and

$$\Psi_T = \hat{h}^{1/2}(x) \int_{-\infty}^{\infty} Q_T(m, k^-) \exp[i(mx + k^- y - \omega t)]dm$$

where Ψ_T and Ψ_R are to be obtained as functions of the incident spectrum by matching sea level, η, and longshore transport, $hv = \Psi_x$, at the jump so as to ensure that the flux of energy, $\frac{1}{2}\rho ghv\eta$, is there continuous. From (6.2), the latter condition implies

$$Q_I + Q_R = s^{1/2} Q_T \tag{6.3}$$

while to match sea level we need only match its gradient, $\eta_x = (gh)^{-1}[\Psi_{yt} + f\Psi x]$, assuming $\eta \to 0$ as $x \to \infty$, so that

$$[\omega k^- + f(b + im)]Q_I + [\omega k^+ + f(b + im)]Q_R = s^{-1/2}[\omega k^- + f(b + im)]Q_T. \tag{6.4}$$

The expressions (6.3) and (6.4) may be immediately rearranged to obtain

$$Q_T = T^{1/2}(m, \omega) e^{-im\Delta x} Q_I \tag{6.5}$$

where

$$T = 4s[(1 + s)^2 + (m/b\gamma)^2(1 - s)^2]^{-1} \tag{6.6}$$

plays the role of a transfer function and

$$m\Delta x = \tan^{-1}[m(b\gamma)^{-1}(1 - s)/(1 + s)] \tag{6.7}$$

represents the cross-shelf displacement of streamlines across the jump. The parameter γ is given by

$$\gamma = [1 - \omega^2 \sigma^{-2}]^{1/2} \tag{6.8}$$

and is real for the spectrum of propagating incident waves assumed while the net transmitted energy flux may be determined from (6.5) and (2.17) and written as

$$F_T = -\rho\pi \int_{-\infty}^{\infty} [\omega k^- + bf] T Q_I Q_I^* dm. \tag{6.9}$$

To "flesh out" the above solutions, we consider the scattering of a single incident wave of the form

$$\Psi_I \approx h^{1/2} \sin(m_I x) \exp[i(k^- y - \omega t)] \tag{6.10}$$

for which the spectrum Q_I is strongly peaked at $\pm m_I$ and approximated by $-i[\delta(m - m_I) - \delta(m + m_I)]/2$. The transmitted flux (6.9) may in this case be approximated by

$$F_T \approx T(m_I, \omega) F_I \tag{6.11}$$

so that the function T may be interpreted as simply the ratio of transmitted to incident energy flux, F_T/F_I. The properties of the function T defined by (6.6) and (6.8) thus imply that the ratio F_T/F_I will (1) decrease with increasing jump size, where $s = \hat{h}_0/h_0$ may differ appreciably from unity (2) be identical for wave propagation from deep to shallow or shallow to deep water, since T is an identical function of s and s^{-1}, and (3) decrease as the cross-shelf scale m_I^{-1} of the incident wave becomes small compared with that of the topography $b^{-1} = 2h/h_x$. In addition, at low frequencies, where $\omega^2 \ll \sigma^2(m_I)$, both the transfer function T and the streamfunction displacement become independent of ω/f as the parameter γ is nearly constant and equal to one. The transfer function and hence flux ratio F_T/F_I are also a maximum at low frequencies since $T(m, \omega)$ monotonically decreases to zero as ω approaches $\sigma(m_I)$, the frequency of the zero group speed of the incident wave. These results are analogous to the dependencies illustrated in Figs. 5–7 for energy transmission across a jump on a bounded shelf. The correspondence with the frequency dependence illustrated in Fig. 7 is particularly interesting as it suggests that the rectification of the indeterminate flaw in the solution technique applied for bounded shelves should not affect the qualitative nature of the estimated frequency dependence of F_T/F_I.

At low frequencies we expect waves to propagate along f/h contours which suffer a displacement, $\Delta x_T = -(2b)^{-1} \ln(s)$, as the jump is crossed. Indeed, inspection of (6.7) shows this to be the case, $\Delta x \approx \Delta x_T$, provided that the cross-shelf scale m_I^{-1} is of order or larger than $b^{-1} = 2h/h_x$ and $s = \hat{h}/h$ lies in the range 0.5 to 2. Where the incident wave scale m_I^{-1} is small compared with b^{-1} the streamline displacement is less than that required to follow f/h contours and, as noted above, the transmitted flux is small.

The preceding comments on transmitted flux are in

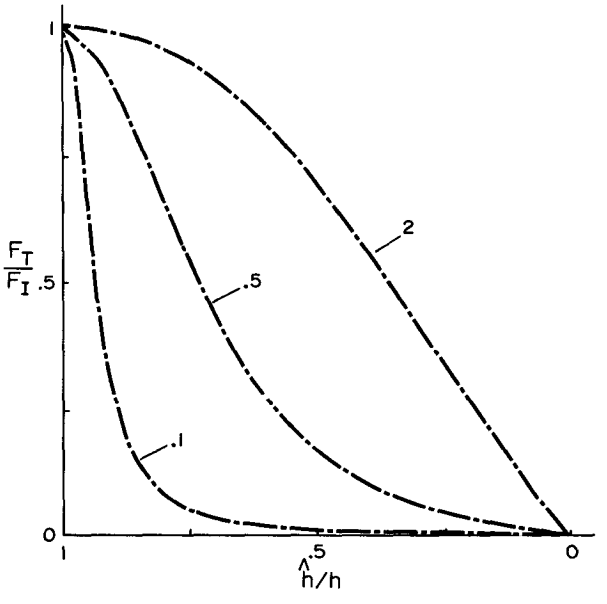

FIG. 8. Ratio of transmitted to incident energy flux F_T/F_I vs jump size $s = \hat{h}_0/h_0$ for a narrow band low frequency, incident wave spectrum centered on m_I. Results, obtained from (3.6), are presented for the slope parameter, bL, indicated and the first mode wavenumber, $m_I = \pi L^{-1}$, that formally correspond to a wall at $x = L$.

part summarized in Fig. 8 where the ratio F_T/F_I given by (6.11) is plotted against jump size for low frequencies where γ is near unity. Results were obtained using three values of the slope parameter bL, (0.1, 0.5 and 2.0), and the first mode wavenumber, $m_I = \pi/L$, that formally corresponds to a wall at $x = L$. We note that while the results in Fig. 8 are qualitatively similar to those presented in Fig. 5, the results for an unbounded shelf do show significantly reduced transmission compared to those obtained for a bounded shelf. This quantitative difference might have been expected as the relative change in depth indicated by the abscissa in Fig. 8 is uniform in x, whereas that in Fig. 5 corresponds to the maximum depth change across the shelf.

b. Results for a smooth topographic jump

The preceding results presented here are strictly valid only for the case of an abrupt jump in bottom topography. In reality, such a situation rarely, if ever, occurs in the ocean so it is of interest to consider the parameter range over which a smooth change in topography may be reasonably represented by an abrupt jump. To examine this question, we consider results for the following topography:

$$h = \begin{cases} h_0 \exp(2bx), & y \geq 0 \\ h_0 \exp(2bx + 2cy), & -a \leq y \leq 0 \\ \hat{h}_0 \exp(2bx), & y \leq -a \end{cases} \quad (6.12)$$

where $\hat{h}_0 = h_0 \exp(-2ca)$. In the regions $y \geq 0$, and $y \leq -a$, solutions are again of the form given above by (6.2) since h is a function of x only. Within the region $-a \leq y \leq 0$, h is a function of both x and y so that the vorticity equation (2.2) is replaced by

$$\frac{\partial}{\partial t}(\nabla^2\Psi - 2b\Psi_x - 2c\Psi_y) + 2f(b\Psi_y - c\Psi_x) = 0$$

which allows solutions of the form

$$\Psi = h^{1/2}(x, y) \int_{-\infty}^{\infty} \{Q^-(m, k^-) \times \exp[i(mx + k^- y - \omega t)] + Q^+(m, k^+) \exp[i(mx + k^+ y - \omega t)\} dm \quad (6.13)$$

where k^- and k^+ are now determined from the dispersion relation

$$(m - fc/\omega)^2 + (k + fb/\omega)^2 = (b^2 + c^2)(f^2\omega^{-2} - 1).$$

As indicated by (6.13), both long and short waves are present in the transition region, $-a \leq y \leq 0$, due to reflection at $y = -a$.

The general solution is now easily determined by matching transport and sea level across y = 0 and $-a$. The solution for $y \leq -a$ may be written as

$$Q_T = T_s^{1/2}(m, \omega) e^{-i\theta} Q_I \quad (6.14)$$

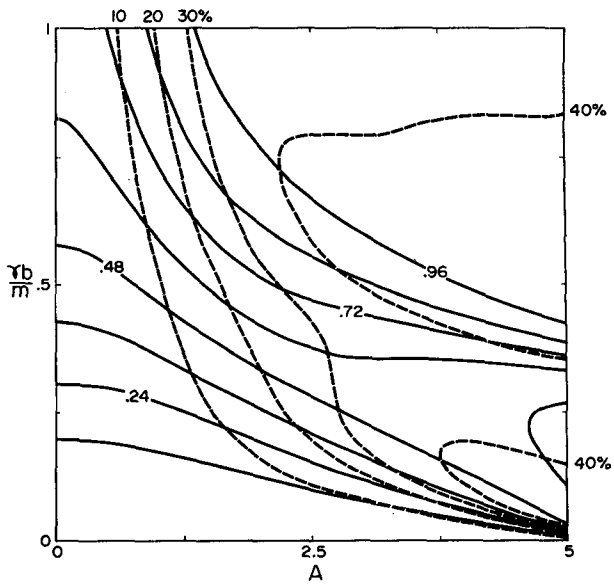

FIG. 9. Contour of the flux ratio F_T/F_I given by (6.20) for a smooth topographic jump where $ca = \frac{1}{2}\ln(h_0/\hat{h}_0) = \pm\frac{1}{2}$. Also plotted is the percentage difference between F_T/F_I and that for an abrupt jump where the longshore topographic scale a, and hence $A = -(ma)(ca)f/\omega$ is zero.

where

$$T_s = \left[\cos^2\Delta_1 + \left(\frac{\Delta_2}{\Delta_1}\right)^2 \sin^2\Delta_1\right]^{-1} \quad (6.15)$$

$$\Delta_1 = i\left[(ca)^2 - \left(\frac{b\gamma}{cam}\right)^2 A^2 - 2A\right]^{1/2} \quad (6.16)$$

$$\Delta_2 = \left[\left(\frac{b\gamma}{cam}\right)A + \left(\frac{b\gamma}{cam}\right)^{-1}\right] \quad (6.17)$$

$$\theta = \tan^{-1}(\Delta_2\Delta_1^{-1} \tan\Delta_1) + A\left(\frac{b\gamma}{mca}\right) \quad (6.18)$$

$$A = -(ma)(ca)f/\omega. \quad (6.19)$$

The transfer function (6.15) and phase shift (6.18) now involve two new parameters A and ca, where the latter is, by (6.12), a measure of the jump size, $ca = \frac{1}{2}\ln(h_0/\hat{h}_0)$, and equal to the total displacement $b\Delta x_T$ of f/h contours across the smooth jump. The parameter A is proportional to the longshore extent of the jump region and as A vanishes the transfer function (6.15) and phase shift asymptote to those found for an abrupt jump.

To compare the wave scattering implied by (6.14)–(6.19) with results for an abrupt jump, we consider an incident wave of the form (6.10), so that Q_I is narrow band about $\pm m_I$ and implies a transmitted flux of

$$F_T = \frac{1}{2}[T_s(m_I, \omega) + T_s(-m_I, \omega)]F_I. \quad (6.20)$$

A plot of the ratio F_T/F_I is contoured in Fig. 9 for the large jump, $ca = \pm 0.5$ or $\hat{h}_0/h_0 = (2.72)^{\pm 1}$. The param-

eter $\gamma b/m_I$ is chosen to vary from zero to one so as to include typical values. The parameter, $A = -(m_I a)(ca) \times f/\omega$, is chosen to vary from zero, (an abrupt jump), to five so as to allow for a jump transition region, a, that is of order the shelf width, for $\omega \sim -0.2f$ and $m_I L \sim 2$. Plotted also in Fig. 5 is the percentage error between the smooth topography flux estimates contoured and those obtained for an abrupt jump, where A is zero.

The results show the abrupt model flux (6.6) to be within 20% of (6.20) provided that $\gamma b/m_I$ and A are respectively less than ½ and 2. Such a parameter space is not overly restrictive as $\gamma b/m_I$ is typically ½ or less, while for $\omega/f = -0.2$ and $m_I L \sim 2$, the condition $A < 2$ admits a transition region a, that is up to 0.4 shelf widths in length. For a smaller jump, $ca = \pm 0.1$, results analogous to Fig. 9 may be determined which show that the flux estimated for an abrupt jump will again be within 20% of those obtained for $A < 2$. Here however, since ca is one-fifth of the value above, the corresponding transition region is equal to two shelf widths. We note also that the permitted transition region will become larger at higher frequencies as both $\gamma b/m_I$ and A then become smaller. These results suggest then that the bounded shelf results may apply in a qualitative sense to the scattering by smooth jumps where the length of the transition region is of order one-half or less of the shelf width.

The condition that A be less than 2 here is analogous to that established by Rhines (1969) for the propagation of planetary Rossby waves over abrupt topography. (Note that in his paper ω/δ should be replaced by δ/ω in the third and fourth lines of pages 171 and 172 respectively.) Indeed, the results of this section are, in general, analogous to those presented by Rhines with fh_x/h playing the role of β.

7. Summary and discussion

The scattering of barotropic shelf waves by abrupt longshore jumps in topography was examined for bounded and unbounded exponential shelves by matching modal and spectral representations for sea level and longshore transport.

At low frequencies it was shown that solutions for the total streamfunction, ϕ, may be obtained from the differential equation.

$$(1/h - 1/\hat{h})\phi_x = 2b(\phi - \phi_I)/h \qquad (3.5)$$

which, as shown, represents the change in, or production of, relative vorticity in the form of reflected waves (the right-hand side) due to vortex stretching induced by flow over the jump in depth (the left-hand side). When all f/h contours in the backward region are continued across the jump in topography, (3.5) yields solutions which are shown (for abrupt changes in depth and width) to agree with those obtained by direct mode-matching techniques: no solutions were obtained where f/h contours in the backward region were not continued across the jump. For each case considered, incident wave energy is predominantly scattered into transmitted and reflected waves, with cross-shelf structures similar to that of the incident wave. In addition, all scattered waves were either in or out of phase with the incident wave since their amplitudes a_j, $\hat{a}_j$ are determined from the real differential equation (3.5) and modal functions ϕ_j, $\hat{\phi}_j$. Streamlines were also found to follow f/h contours resulting in a quiescent or shadow zone forward of the topographic jump.

Surprisingly, for the case of a jump in depth the inclusion of evanescent modes in a direct mode-matching approach did not result in accurate solutions for the case where f/h contours are not continued into the forward region. Further, the mode-matching technique failed to give accurate, energy-conserving solutions at higher frequencies even in the case where f/h contours are continued into the forward region. In contrast to the analyses of Wilkin and Chapman (1987), the inclusion of the Kelvin wave mode did not reduce the errors in total energy flux suggesting there to be some basic problem in either the mode-matching techniques tried or in the assumed physics. It is possible that in the cases where energy is not conserved, wave propagation across the topographic jump is necessarily accompanied by loss of energy from the nondivergent wave field either through frictional dissipation or through the (nonlinear) transfer of energy to inertia–gravity waves and a "mean" current [Haidvogel and Brink (1986) give an interesting discussion of the generation of mean currents by the latter process]. In the absence of these processes there may be no solutions of the periodic form assumed here. Examination of numerical model results could clearly shed light on the foregoing conjectures.

In spite of the uncertainties discussed, it should be noted that the solutions obtained by matching modal representations of Ψ and η_x did agree with those obtained from (3.5) at low frequencies, and although only approximate solutions were obtained at higher frequencies, the resulting estimates of the transmitted to incident energy flux ratio, F_T/F_I, were in qualitative agreement with the exact solutions obtained for an unbounded shelf.

In fact, for an unbounded shelf with constant jump size, $s = \hat{h}/h$, solutions are easily found for all cases, and F_T/F_I has been shown to be given by

$$T = 4s[(1 + s)^2 + (m_I/b\gamma)^2(1 - s)^2]^{-1} \qquad (6.6)$$

for an incident wave of the form $\Psi_I \approx h^{1/2} \sin(m_I x) \times \exp[i(k^- y - \omega t)]$. The result (6.6) implies that the ratio F_T/F_I will decrease with increasing jump size and be identical for waves which propagate from deep to shallow or shallow to deep water since $T(s) = T(s^{-1})$. In addition, the ratio of fluxes given by (6.6) is a maximum at frequencies for which ω^2 is much less than that of the zero in incident wave group speed, σ_I^2, since

$\gamma = (1 - \omega^2 \sigma_I^{-2})^{1/2}$ is then near one. At such low frequencies, waves were also found to propagate along f/h contours, even as the jump is crossed, provided that the cross-shelf wave scale m_I^{-1} is larger than that of the topography $b^{-1} = 2h/h_x$. However, for high 'mode' waves, where m_I^{-1} is small compared with b^{-1}, the displacement of streamlines was found to be less than that required to follow f/h contours and the transmitted flux much reduced. At higher frequencies, the parameter γ and ratio F_T/F_I given by (6.6) both monotonically decreases to zero as the frequency σ_I is approached.

Estimates of wave scattering by smooth topographic variations were also obtained by assuming the shelf to be unbounded in the on/off-shore directions. In brief, the ratios of F_T/F_I obtained for smooth and abrupt jumps were found to differ by less than 20% for low mode, low frequency waves and longshore transition regions less than about a half shelf width. At higher frequencies, the "permitted" longshore transition region will be larger. These results should apply in a crude sense to the scattering on bounded shelves since results obtained for the scattering by an abrupt jump on both bounded and unbounded shelves are qualitatively similar. Indeed, the general conclusions obtained from the abrupt jump analysis here are supported by the bounded shelf results of Webster (1987) who considered the scattering due to smooth self-similar changes in shelf width and depth. In qualitative agreement with the analysis here, he finds, using mode matching techniques, that the transmitted energy decreases with the length of the transition region and that severe scattering does occur when this length is less than one half of the shelf width. In addition, Webster also shows that most energy is scattered into the gravest propagating modes and that the longshore topographic variations act to low pass filter incident wave energy in both frequency and mode number spaces.

The results presented are of course strictly applicable only to a barotropic ocean. Huthnance (1978) has shown that stratification generally increases the phase speed of each mode. Further, Chapman (1983) demonstrates that if the maximum value of Nh_x/f, evaluated along the bottom (N is the Brunt–Väisälä frequency), exceeds one then ω reaches f at a finite wavenumber for each mode: no zero group velocity points exist and consequently no shelf wave modes capable of transporting energy in the backward direction exist. Thus, while the qualitative nature of solutions for an abrupt increase in shelf width (where no backscattering occurs) will not likely be changed by the effects of stratification, the results for an abrupt change in depth (where backscattering is typically strong) are expected to be substantially modified unless stratification is weak.

The present study was motivated by the desire to model wave propagation down the Labrador Shelf where the wintertime stratification is believed to be very weak. Even in this case quantitative details are not expected to be accurate and qualitative conclusions require verification. The results do, however, suggest that wave scattering is important in this region. In view of the demonstration by Brink (1986) that topographic scattering of coastal trapped waves is not generally weakened by the inclusion of stratification, it is unlikely that this qualitative conclusion will be negated by the inclusion of stratification.

Finally, we note that the difficulties encountered in our attempts to determine barotropic solutions using a straightforward mode-matching approach are likely to be encountered in stratified models as well. It would seem prudent to examine barotropic models further in order to resolve the questions raised in the simplest possible context.

Acknowledgments. Comments and constructive criticisms by two anonymous reviewers have significantly influenced the presentation and discussion of results.

REFERENCES

Allen, J. S., 1976: Continental shelf waves and alongshore variations in bottom topography and coastline. *J. Phys. Oceanogr.*, **6**, 864–878.

Brink, K. H., 1980: Propagation of barotropic continental shelf waves over irregular bottom topography. *J. Phys. Oceanogr.*, **10**, 765–778.

——, 1986: Scattering of long coastal-trapped waves due to bottom irregularities. *Dyn. Atmos. Oceans*, **10**, 149–164.

Buchwald, V. T., and J. K. Adams, 1968: The propagation of continental shelf waves. *Proc. Roy. Soc. London*, **A305**, 235–250.

Chao, S.-Y., L. J. Pietrafesa and G. S. Janowitz, 1979: The scattering of continental shelf waves by an isolated topographic irregularity. *J. Phys. Oceanogr.*, **9**, 687–695.

Chapman, D. C., 1983: On the influence of stratification and continental shelf and slope topography on the dispersion of subinertial coastally trapped waves. *J. Phys. Oceanogr.*, **13**, 1641–1652.

Davis, A. M. J., 1983: Shelf similar topographies for free continental shelf waves. *Geophys. Astrophys. Fluid Dyn.*, **23**, 321–331.

Haidvogel, D. B., and K. H. Brink, 1986: Mean currents driven by topographic drag over the continental shelf and slope. *J. Phys. Oceanogr.*, **16**, 2159–2171.

Hsueh, Y., 1980: Scattering of continental shelf waves by longshore variations in bottom topography. *J. Geophys. Res.*, **85**, 1147–1150.

Huthnance, J. M., 1978: On coastal trapped waves: Analysis and numerical calculations by inverse iteration. *J. Phys. Oceanogr.*, **8**, 74–92.

Rhines, P. B., 1969: Slow oscillations in an ocean of variable depth. Part I. Abrupt topography. *J. Fluid Mech.*, **37**, 161–189.

Wang, D.-P., 1980: Diffraction of continental shelf waves by irregular alongshore geometry. *J. Phys. Oceanogr.*, **10**, 1187–1199.

Webster, I., 1987: Scattering of coastally-trapped waves by changes in shelf width. *J. Phys. Oceanogr.*, (in press).

Wilkin, J. L., and D. C. Chapman, 1987: Scattering of continental shelf waves at a discontinuity in shelf width. *J. Phys. Oceanogr.*, (in press).

Yeh, H.-C., 1975: Method of solving potential field problems with complicated geometries. *J. Appl. Phys.*, **46**, 4431–4440.